Fundamental Behavior of Piezoceramic Sheet Actuators

JAYANT SIROHI AND INDERJIT CHOPRA*
Alfred Gessow Rotorcraft Center, Department of Aerospace Engineering, University of Maryland, College Park, MD 20742

ABSTRACT: This paper investigates the behavior of piezoceramic sheet actuators under different types of excitation and mechanical loading. The research especially focuses on the application of these actuators to the development of smart rotor systems. The free strain response of the actuators under DC excitation is experimentally investigated along with the associated drift of the strain over time. Effect of tensile stress on the free strain response is examined. The magnitude and phase of the free strain response of the actuator under different excitation voltages and frequencies is measured, and a phenomenological model to predict this behavior is developed and validated. The power consumption of the free actuator and a pair of actuators surface bonded to a host structure is calculated by the impedance method and validated by measurement. Additionally, depoling of the actuators is discussed, along with the feasibility of recovering performance by repoling in the event of accidental depoling.

INTRODUCTION

PIEZOCERAMICS are potential actuators for a wide range of applications in aerospace, automotive, civil structures, machine tools and big-medical systems to actively control vibration and noise, improve performance, and augment stability. One of the major barriers for various applications is the stroke of these actuators (Chopra, 1996). To increase induced strain, these actuators are often driven under high electric fields, and sometimes even to extreme limits. In addition to this, the operating condition of the system itself may cause high mechanical loads on the actuator. For example, in rotorcraft applications, actuators placed on rotor blades are exposed to high tensile stresses due to centrifugal forces (Chopra, 1997). Though the piezoelectric material is relatively well behaved and linear at low electric fields and low mechanical stress levels, it shows considerable nonlinearity at high values of electric field and mechanical stress. In order to develop an efficient structural system with piezoceramic actuators, it is necessary to accurately predict the response of the actuators, including magnitude and phase of induced strain, power consumption and integrity under different excitation and loading levels. Currently, mathematical tools to cover a wide range of operating conditions along with reliable test data to validate these tools are not available.

The most commonly used type of piezoceramics, Lead Zirconate Titanates (PZTs) are solid solutions of lead zirconate and lead titanate, often doped with other elements to obtain specific properties. These ceramics are manufactured by mixing together proportional amounts of lead, zirconium and titanium oxide powders and heating the mixture to around 800–1000°C. They then react to form the perovskite PZT powder. This powder is mixed with a binder and sintered into the desired shape. During the cooling process, the material undergoes a paraelectric to ferroelectric phase transition and the cubic unit cell becomes tetragonal. As a result, the unit cell becomes elongated in one direction and has a permanent dipole moment oriented along its long axis (*c*-axis). A typical PZT unit cell is shown in Figure 1. A volume of the material in which the polar moments of the unit cell are all oriented in the same direction is called a domain. The unpoled ceramic consists of many randomly oriented domains and thus has no net polarization.

Application of a high electric field has the effect of aligning most of the domains in such a way that the polar axes of the unit cells are oriented as closely parallel to the applied field as allowed by the crystal structure. This process is called poling and it imparts a permanent net polarization to the ceramic. Since the polar axis (*c*-axis) of the unit cell is longer than the other two axes (*a*, *b*-axes), the reorientation of the domains also creates a permanent mechanical distortion. The polar axes can be reoriented in certain specific directions governed by the crystal symmetry in the presence of a high electric field or mechanical stress. This process is called switching. In the case of tetragonal PZTs, either 90° or 180° switching can occur. The 90° switching is always accompanied by mechanical distortion due to the longer length of the unit cell along the polar axes, while the 180° switching can occur without any distortion. It is also known that an electric field can cause both 180° and 90° domain switching but a mechanical stress can only cause 90° switching. Consequently, a mechanical stress can depole a piezoelectric ceramic but cannot repole it. The poled ceramic exhibits the direct and converse piezoelectric effects. The converse effect is the deformation of the piezoceramic in response to an electric field

*Author to whom correspondence should be addressed. E-mail: chopra@eng.umd.edu

1530-8138/00/01 0047-15 $10.00/0 DOI: 10.1106/WV49-QP37-4Q1M-P425

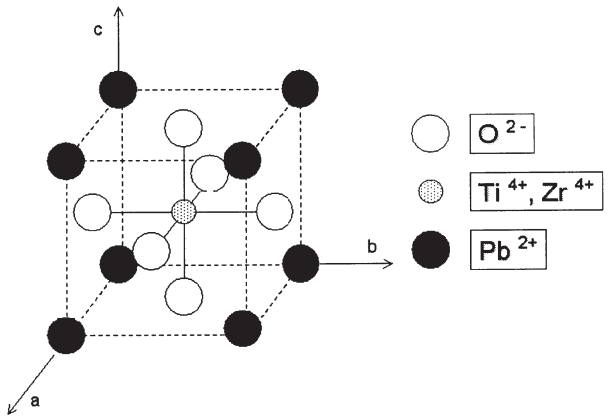

Figure 1. *Typical PZT unit cell.*

and there are three main phenomena causing it. The first one is the piezoelectric effect of the aligned domains. This is the deformation of the unit cell caused by the electric field and is also called the intrinsic effect. The second one is as a result of deformations caused by non-180° domain wall motion and related phenomena. These effects are also called extrinsic effects. Li et al. (1991) have presented evidence to show that extrinsic effects are the major cause of non-linearity and losses in the piezoceramic. The intrinsic contribution to such losses is small. The third one is the electrostriction effect. The electrostrictive deformation is proportional to the square of the electric field and is independent of the direction of the field. The relation between the field and deformation is centrosymmetrical, in contrast to the piezoelectric effect, which is noncentrosymmetrical. The electrostrictive effects are usually much smaller than the other two effects.

Constitutive Relations

Under small field conditions, the constitutive relations for a piezoelectric ceramic are (IEEE Standard, 1987):

$$D_i = e_{ij}^{\sigma} E_j + d_{im}^{d} \sigma_m \tag{1}$$

$$\varepsilon_k = d_{jk}^{c} E_j + s_{km}^{E} \sigma_m \tag{2}$$

where vector D_i of size (3×1) is the electric displacement, ε_k is the strain vector (6×1), E_j is the applied electric field vector (3×1) and σ_m is the stress vector (6×1). The piezoelectric constants are the dielectric permittivity e_{ij}^{σ} of size (3×3), the piezoelectric coefficients d_{im}^{d} (3×6) and d_{jk}^{c} (6×3), and the elastic compliance s_{km}^{E} of size (6×6). The superscripts c and d have been added to differentiate between the converse and direct piezoelectric effects, though in practice, these coefficients are numerically equal. The superscripts σ and E indicate that the quantity is measured at constant stress and constant electric field respectively. The poling direction, which is along the thickness, is denoted as the 3-axis. The 1-axis and 2-axis are in the plane of the piezoceramic sheet. The material is normally assumed transversely isotropic in the 1-2 plane. The d_{jk}^{c} matrix can then be expressed as

$$\mathbf{d} = \begin{bmatrix} 0 & 0 & d_{31} \\ 0 & 0 & d_{31} \\ 0 & 0 & d_{33} \\ 0 & d_{15} & 0 \\ d_{15} & 0 & 0 \\ 0 & 0 & 0 \end{bmatrix} \tag{3}$$

where d_{31} and d_{33} relate the normal strain in the 1 (or 2) and 3 directions respectively to a field along the poling direction, E_3, while d_{15} relates the shear strain in the 2-3 and 1-3 planes to the transverse fields, E_1 and E_2. Note that there is no shear in the 1-2 plane. For PZT-5H, $d_{31} = d_{32}$ and the material is considered transversely isotropic as far as piezoelectric properties are concerned, whereas a material like Polyvinylidene Flouride (PVDF) is piezoelectrically orthotropic. The compliance matrix is of the form

$$\mathbf{s} = \begin{bmatrix} S_{11} & S_{12} & S_{13} & 0 & 0 & 0 \\ S_{12} & S_{22} & S_{13} & 0 & 0 & 0 \\ S_{13} & S_{13} & S_{33} & 0 & 0 & 0 \\ 0 & 0 & 0 & S_{44} & 0 & 0 \\ 0 & 0 & 0 & 0 & S_{44} & 0 \\ 0 & 0 & 0 & 0 & 0 & S_{66} \end{bmatrix} \tag{4}$$

and the permittivity matrix is

$$\mathbf{e}^{\sigma} = \begin{bmatrix} e_{11}^{\sigma} & 0 & 0 \\ 0 & e_{11}^{\sigma} & 0 \\ 0 & 0 & e_{33}^{\sigma} \end{bmatrix} \tag{5}$$

Equation (1) is the sensor equation and Equation (2) is the actuator equation. Sensor applications are based on the direct effect. On the application of a constant stress, and under conditions of zero electric field, Equation (1) becomes

$$D_i = d_{im}^{d} \sigma_m \tag{6}$$

The electric displacement D is related to the generated charge by the relation

$$q = \int\int D dA \tag{7}$$

where dA is the infinitesimal area normal to the displacement D. The charge q (Coulombs) and the voltage generated across the sensor electrodes are related by the capacitance of the sensor; $V = q/C$. It should be noted that measurement of piezoelectric coefficients by the direct effect is usually more difficult and less accurate than measurement based on the converse effect. This is because application of a pure uniaxial

stress is difficult and some of the charge generated by the application of stress can leak off before it is measured. On the other hand, while using the converse effect, it is much easier to apply a uniform electric field and assure a zero stress state within the sample. It is also difficult to control the electrical boundary conditions during static testing. However, static measurements are made more accurate by superimposing a low frequency alternating electric field or mechanical stress.

SAMPLE PREPARATION AND CYCLING

The actuators investigated in all the experiments described below were piezceramic (PZT-5H) sheets of dimension $1'' \times 0.5'' \times 0.01''$ obtained from Morgan Matroc Inc. (Morgan Matroc, 1993). Some of the manufacturer supplied characteristics of this material are shown in Table 1. All the samples were poled along their thickness. They were excited along the poling direction and strains were measured in a plane perpendicular to the poling direction. Each sample was instrumented with a strain gage with a gage length of 0.125″ in a quarter bridge configuration. The excitation leads were soldered to the faces of the sheet and the sample was suspended by means of the excitation leads, so there is no structural boundary constraint. The experimental data shown below represents the average behavior of three randomly selected samples for each test. Before the tests were carried out, the samples were cycled to erase the effect of previous excitations. The cycling can be of two types, depending on whether the properties to be observed are static or dynamic.

If the application involves a static excitation, a DC cycling is performed on the actuator. This involves exciting the actuator with its highest operating DC field, switching off the field, and then measuring the residual strain. This process is repeated several times until the residual strain after each cycle has stabilized. A schematic of the actuator strain during the DC cycling process is shown in Figure 2. After each cycle, the residual strain keeps decreasing until it becomes almost zero. The number of cycles needed to stabilize the performance depends on the cycling field and normally increases with increasing cycling field. A cycled actuator has an inherent bias and will show almost zero residual strain on the application of an excitation field less than the cycling field. Note that the polarity of the field is important and that reversing the polarity, either during cycling or during operation of the acutator, will destroy the bias. This treatment is therefore suitable only for unipolar operations. If the actuator is exposed to the DC cycling voltage for a long period of time, it is observed that there is an additional effect of stabilizing the drift, as will be discussed later. Another type of cycling treatment is AC cycling which involves exciting the actuator for several cycles under an AC field. The effect of this treatment is that it removes all biases in the actuator and also minimizes residual strain.

Table 1. Small signal PZT-5H characteristics.

d_{31}	-274×10^{-12} m/V
d_{33}	593×10^{-12} m/V
d_{15}	741×10^{-12} m/V
s_{11}^E	16.5×10^{-12} m²/N
s_{33}^E	20.7×10^{-12} m²/N
s_{44}^E	43.5×10^{-12} m²/N
s_{12}^E	-4.78×10^{-12} m²/N
s_{13}^E	-8.45×10^{-12} m²/N
ρ	7500 kg/m³
Curie point	193°C
K_{11}^σ	3130
K_{33}^σ	3400
Compressive strength	>75,000 psi
Static tensile strength	~11,000 psi
Poling field	~12 kV/cm
Dielectric breakdown	~20 kV/cm
Depoling field (DC)	~5.5 kV/cm

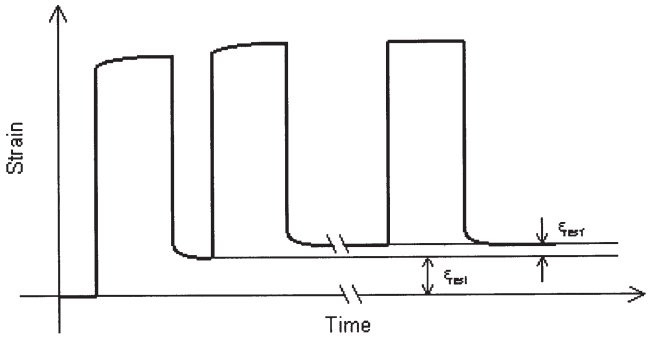

Figure 2. *Strain during DC cycling.*

STATIC BEHAVIOR

Static Free Strain

A typical DC field (along the polarized direction) versus transverse free strain (in a plane normal to the polarized direction) plot for a PZT-5H actuator is shown in Figure 3. To obtain the static free strain plot, the following steps were taken. DC cycling is initially carried out on the sample to minimize its residual strains. A typical sample required on the order of 10 DC cycles to bring the residual strain to less than 3 με. Each point on the curve is then obtained by applying a DC field and measuring the resulting strain with a strain gage. After each reading, the excitation is switched off and the gage is reset. This effectively ignores the hysteresis and drift and generates a quasi-steady free strain curve. The curve is almost linear at low applied electric field levels and the linear piezoelectric coefficients can be used to satisfactorily predict this part of the curve. In this region, the slope of the curve is the coefficient d_{31} and the value quoted by the manufacturer (Morgan Matroc, 1993) is -274×10^{-12} m/V. The strains predicted by this linear relation are also plotted for comparison. The negative value of d_{31} means that a positive electric field in the polarization direction results in a compressive strain on the surface of the PZT sheet. At higher electric fields, nonlinear effects become apparent. These ef-

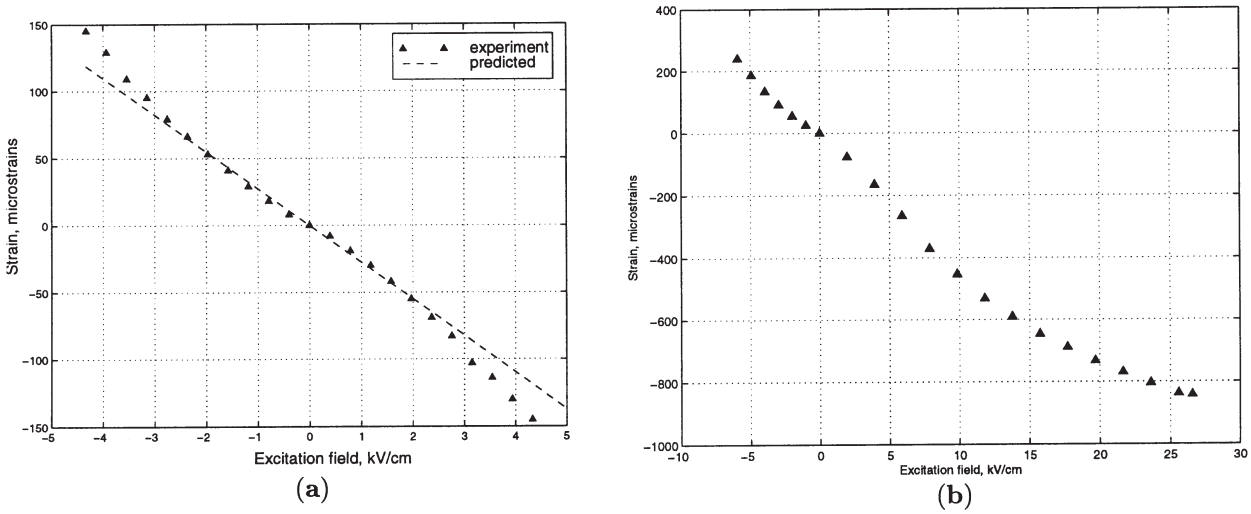

Figure 3. *Static free strain behavior of PZT-5H: (a) low excitation levels and (b) high excitation levels.*

fects are attributed to effects like reversible domain wall motion. The reason that such effects are much smaller at lower values of electric field is that non-180° domain wall motion results in a permanent mechanical distortion of the material and consequently requires a larger energy, and hence, occurs at larger field strengths. At high field strengths, a larger change in induced strain per unit increase in field is expected, both for negative and positive fields. Also, strain values for the same positive and negative fields are not equal, which means the free strain curve is asymmetric. Such an asymmetry has also been observed in the inverse piezoelectric response of Rochelles salt (Vigness, 1935) and is attributed to the permanent electric polarization in the crystal. The asymmetry present in piezoceramics is small for low values of field but becomes larger as the field is increased. In terms of actual voltage applied to the piezoceramic sheet, a voltage of 100 Volts corresponds to a field of 3.937 kV/cm. The data plotted represents the average of 3 separate trials on each of 10 different samples. While testing piezoceramics, such an averaging process is essential to obtain consistent data since there usually may be scatter in the properties of individual samples.

Figure 3(b) shows a free strain curve spanning a much higher field range. The maximum positive field is limited by the breakdown of the dielectric, which in this case is the ceramic itself, whereas the maximum negative field is limited by the piezoceramic depoling. It can be seen that the positive field region is relatively linear up to at least 10 kV/cm. It should be noted that the DC depoling field for PZT-5H is approximately –5.5 kV/cm.

Effect of External Stresses

In the literature, investigations have been carried out to examine the effect of external mechanical stresses on the behavior of piezoceramics. However, most of the existing works are focussed on the effect of compressive loads, since many early applications of piezoceramics were in underwater devices where the materials are exposed to high hydrostatic stresses. Some results of the effects of compressive stresses can be found in the works of Brown (1961), Kreuger and Berlincourt (1961) and Kreuger (1967, 1968). Compressive stresses tend to align the *c*-axes of the domains perpendicular to the direction of stress. For example, if the compressive stress acts along the *X*-axis, say in the plane of the sheet, the *c*-axes of the domains are randomly reoriented parallel to the *YZ* plane, which is across the thickness. This destroys some of the initial polarization and thus reduces the net polarization. According to Kreuger (1968), hard ceramics like PZT-8 and PZT-4 experience large changes in piezoelectric coefficients but show good recovery upon removal of the stress. But soft ceramics like PZT-5H show a permanent degradation in properties with stress cycles.

Limited work has been done to see the effect of tensile stress on the behavior of piezoceramics, which is very pertinent to their application in the development of a smart rotor (Chen and Chopra, 1997). Experiments were carried out to observe the effects of tensile loads perpendicular to the poling direction on the free strain. A test fixture was designed to apply tensile loads to a piezoceramic sample while allowing it to strain freely. The ceramic samples tested were $2'' \times 1'' \times 0.01''$ commercially available PZT-5H sheets. Loads were applied to the sample by means of weights suspended from a sliding bracket (Figure 4). The static free strain curves were obtained for different values of applied tensile load. The data obtained from 10 samples was averaged out to obtain the final free strain values. The results are shown in Figure 5. From the plot, it can be seen that there is a slight increase in free strain with an increase in applied tensile load. Though this is a very small increase, the averaging process makes it more likely that this is a phenomenological change rather than experimental scatter. It was not possible to apply stresses higher than 2500 psi because of stress concentration near the end supports and a small amount of bending in the sample

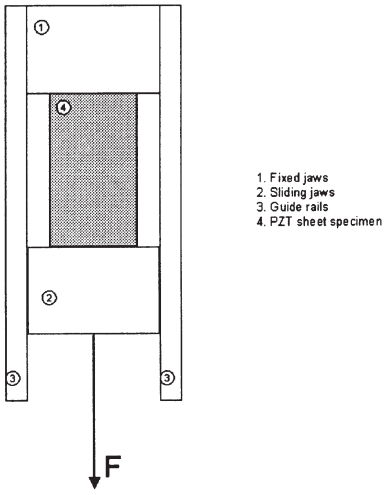

Figure 4. *Tensile testing fixture.*

due to misalignment. Experiments performed by Gerson et al. (1961) show that the static tensile strength of a typical piezoceramic is around 13,000 psi but samples invariably fracture at lower average stresses.

For PZT-5H under a compressive stress parallel to the poling axis (i.e. along the thickness), d_{31} remains constant or shows a slight increase at low values of stress and then drops off at high values of stress (Zhang et al., 1997). Such a stress will tend to randomly reorient the *c*-axes of the unit cells in a plane perpendicular to the poling direction (i.e., in the plane of the sheet). A uniaxial tensile stress acting along the length of the sheet will also tend to align the dipoles along the plane of the sheet, with a preference along the direction of stress. Hence, it can be expected that these two stress states will produce similar changes in properties of the material. Consequently, the behavior seen in Figure 5, with tensile stress in the plane of the piezoceramic sheet is consistent with previously observed phenomena (Zhang et al., 1997) with compressive stress along the poling direction.

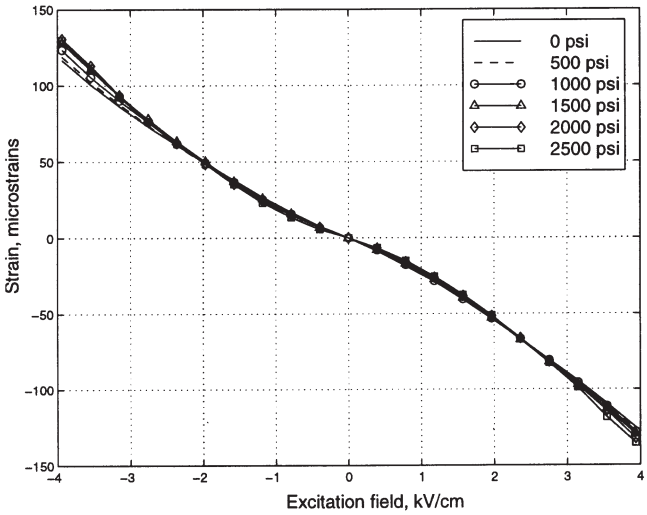

Figure 5. *Variation of static free strain with transverse tensile stress.*

A curve was fit to these data points in order to empirically predict the variation of free strain with applied external stresses. The curve fit was of the form:

$$\varepsilon = a + bE + cE^2 + dE^3 \tag{8}$$

For simplicity, a linear variation of the coefficients *a*, *b*, *c* and *d* with applied tensile stress was fit to the data. This variation is given by:

$$a = -1.9637 - 7.039 \times 10^{-4} P \tag{9}$$

$$b = -25.82 - 7.54 \times 10^{-4} P \tag{10}$$

$$c = -0.1535 + 3.86 \times 10^{-4} P \tag{11}$$

$$d = -0.298 + 1.244 \times 10^{-4} P \tag{12}$$

where ε is the strain in microstrains, *E* is the electric field strength in kV/cm and *P* is the applied tensile stress in psi. As expected, at zero external stress, the free strain curve reduces to that in Figure 3(a). The increase in free strain is of the order of 10% at 3.937 kV/cm under a tensile stress of 2500 psi.

Drift

An effect often observed experimentally is the drift of the actuator strain in response to a DC excitation. The drift phenomenon is a slow increase of the free strain with time after the application of a DC field. An uncontrolled drift in the actuator position is obviously detrimental to the overall performance of systems wherein the actuator is meant to maintain a certain static deflection, for example the steady deflection of a trailing edge flap. The basic drift phenomenon is as follows: after the application of a DC field, the strain jumps to a certain value and then increases slowly with time. When the field is switched off, the strain falls back to some value and then slowly decreases until it stabilizes at some residual strain. The curves describing both the slow increase and the slow decrease are of a similar nature and are roughly logarithmic with time. One of the manufacturers (PI Catalog, 1997) given the following formula for drift of a piezostack actuator:

$$\Delta\varepsilon = \Delta\varepsilon_o \left(1 + \gamma \ln \frac{t}{0.1}\right) \tag{13}$$

where *t* is the time in seconds, $\Delta\varepsilon_o$ is the strain 0.1 seconds after the application of the field and γ is a factor which depends on the system's characteristics, typically of the order of a few percent. Note that the percentage increase in strain after the application of the field is independent of the field strength. Experimental observations on a PZT sheet [Figure 6(a)] shows a family of drift curves for DC excitation fields from

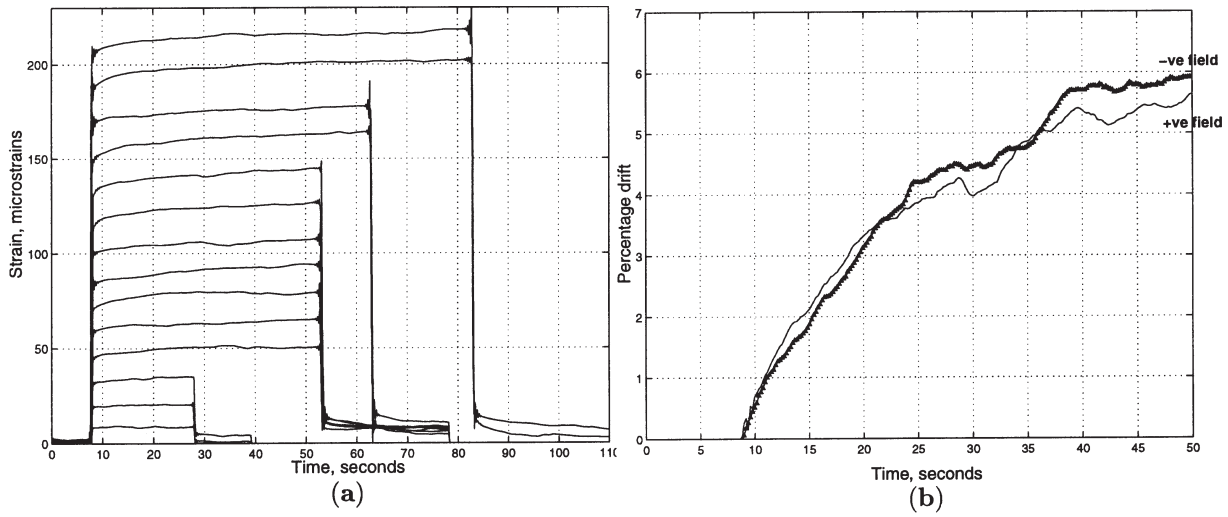

Figure 6. *DC drift behavior: (a) drift in the free strain and (b) effect of field direction.*

0.4 kV/cm to 5.5 kV/cm. The experimental data show that the percentage drift is roughly the same regardless of excitation field. Figure 6(b) shows the percentage drift in response to a positive and a negative field of the same magnitude, 4 kV/cm. It can be concluded that the direction of applied field has negligible effect on the magnitude or the rate of strain drift.

Similar phenomena have been observed by Vigness (1935) during investigations on Rochelle's salt. This gives reason to believe that the drift phenomenon is largely intrinsic in nature. The reason for the drift is probably due to a gradual change in the permanent polarization of the material. Vigness (1935) also showed a dependence of such effects on the state of the material as a result of previous mechanical or electrical treatment, referred to as the "fatigue" effect.

In an attempt to stabilize the drift, an AC field of 5% of the steady DC field was superimposed at high as well as low frequencies. The following five different types of excitations were tried out: (a) 3.937 kV/cm DC field, (b) 0.196 kV_{rms}/cm sinusoidal field at 10 Hz riding on a 3.937 kV/cm DC field, (c) 0.196 kV_{rms}/cm sinusoidal field at 500 Hz riding on a 3.937 kV/cm DC field, (d) 1.968 kV_{rms}/cm sinusoidal field at 500 Hz riding on a 3.937 kV/cm DC field and (e) 3.937 kV/cm DC field on an actuator which was previously exposed to a DC field of the same magnitude for three hours.

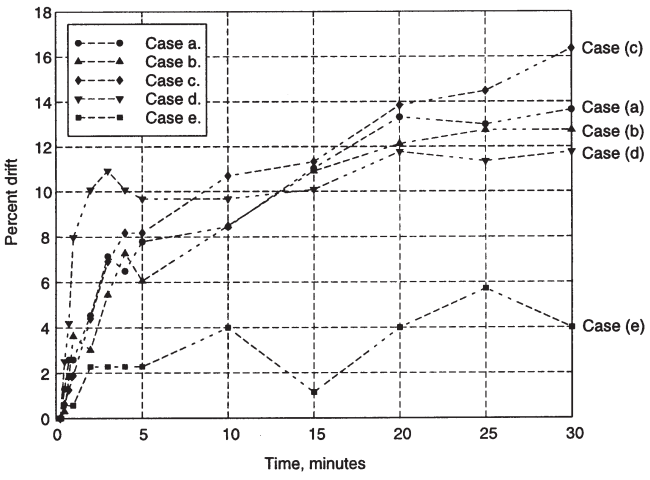

Figure 7. *Drift under combined excitation.*

The effect of these excitations is shown in Figure 7. The percent drift from the instantaneous strain is plotted versus time. After half an hour, the strain signal had increased by approximately 10% to 18%. It can be seen that there is not much change in the drift due to a pure DC field in comparison to those with different superimposed AC fields. The only exception is case (e) where the percent drift is the smallest. The data plotted has been averaged out over three trials. There is some amount of scatter since the repeatability of such drift tests is very sensitive to the previous excitation of the sample. The kind of treatment given to the actuator in case (e) is similar to the fatigue effect, and it appears possible to stabilize drift by exposing the piezoceramic continuously to a DC field for several hours before the actual excitation. It was also observed that the drift is similarly reduced for any excitation field of magnitude less than the stabilization field. This kind of DC stabilization introduces a bias in the piezoceramic and zeros out residual strains in response to an excitation in the same direction. The bias however, is destroyed on reversing the polarity of the field.

DYNAMIC BEHAVIOR

Strain Hysteresis

To observe the losses and the actual hysteretic behavior of the material, a quasi-steady free strain test was performed by changing the voltage successively from point to point. In contrast to the earlier static free strain curve, the excitation was not switched off and the gage was not zeroed after each reading. At each point, the strain was allowed to stabilize be-

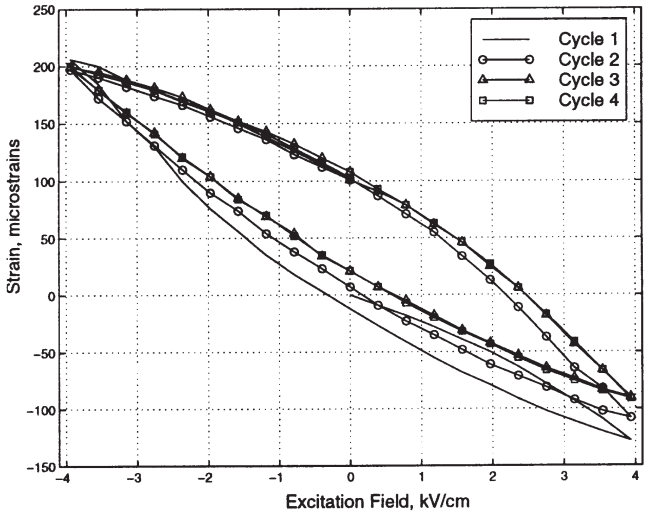

Figure 8. *Quasi-static hysteresis curve, uncycled PZT.*

fore taking a measurement. The experiments were carried out on several different samples and each point is the average of three measurements. The curve shown in Figure 8 was the response of a brand new sample (uncycled). The field was slowly changed in steps of 0.3937 kV/cm. The strain response seems to have some bias and takes around three cycles to stabilize. The same experiment was repeated after exciting the actuator with a moderately high 3.15 kV_{rms}/cm, 5 Hz sinusoidal field. This is referred to as "AC cycling" and is done in an attempt to train the actuator to a certain excitation, such that its residual strain and drift are minimized. The quasi-static strain response, shown in Figure 9(a) now seems to have less bias and stabilizes in the second cycle itself. The aspect ratio (lateral width to length ratio) of the hysteresis curves is around 15%. Figure 9(b) shows the quasi-steady hysteresis curve at a lower maximum field: the aspect ratio becomes smaller. It can be seen that the normalized area under the curve is larger when the maximum field is larger. Also, the curves are asymmetric with respect to the zero strain axis, which is similar to the asymmetry observed in the static free strain curves and is due to the permanent electric polarization of the ceramic. Another interesting feature is that the curves in Figure 9(b) were obtained by starting with a negative excitation whereas the curves in Figure 9(a) were obtained by starting with a positive excitation. This difference is seen in the first quarter of the first cycle. The remainder of the curves show no dependence on the sequence of excitation.

The shape of the strain-field hysteresis loop changes with excitation frequency and field. Figure 10(a) shows the variation in the experimentally measured strain-field hysteresis loop at 5 Hz for a free actuator. It can be seen that with increasing field, the overall shape of the curve is not affected much, but the mean slope increases with increasing field. Also plotted for the sake of comparison is the DC free strain curve, which matches closely with the increasing positive excitation and increasing negative excitation segments of the hysteresis curves. This is to be expected, since the DC free strain curve is obtained from the low frequency strain-hysteresis response by ignoring the hysteresis. The dynamic hysteresis curves reduce to the static free strain curve as the frequency of excitation is decreased. The effect of frequency is seen in Figure 10(b). The area under the high frequency curve is less than the area under the low frequency curve, which means that there are more energy losses at lower frequencies. These hysteresis curves can be generated using the phenomenological model developed above, which also traces out the static free strain curve when the frequency goes to zero.

Dynamic Strain Response

To observe the magnitude and phase of the induced strain of a free actuator under AC excitation, the sample was excited by a sinusoidal field stepped from 0 to 200 Hz. This was

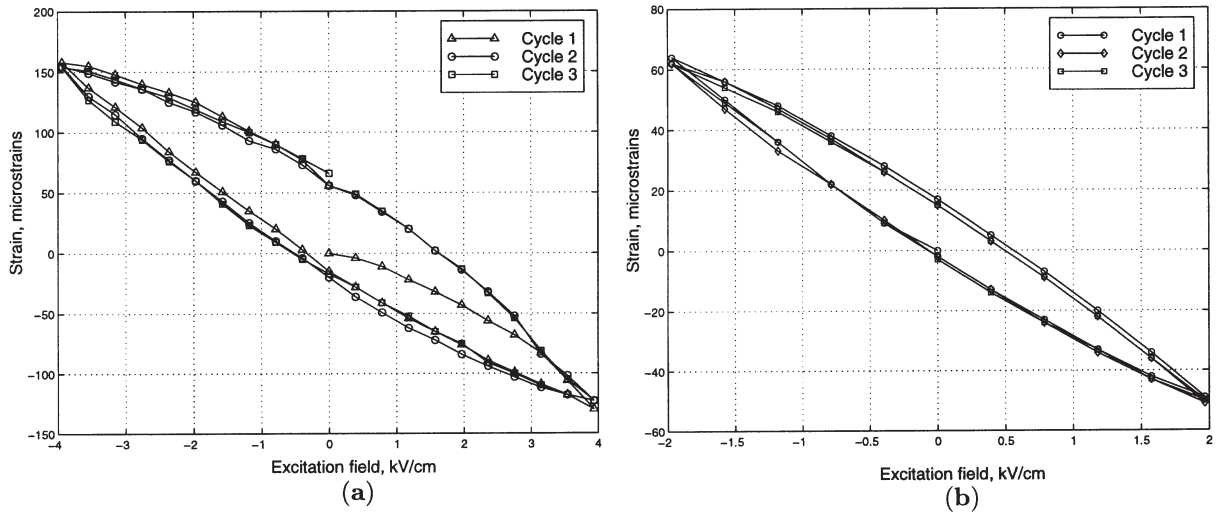

Figure 9. *Quasi-static hysteresis curves, after AC cycling: (a) maximum field = 3.937 kV/cm and (b) maximum field = 1.968 kV/cm.*

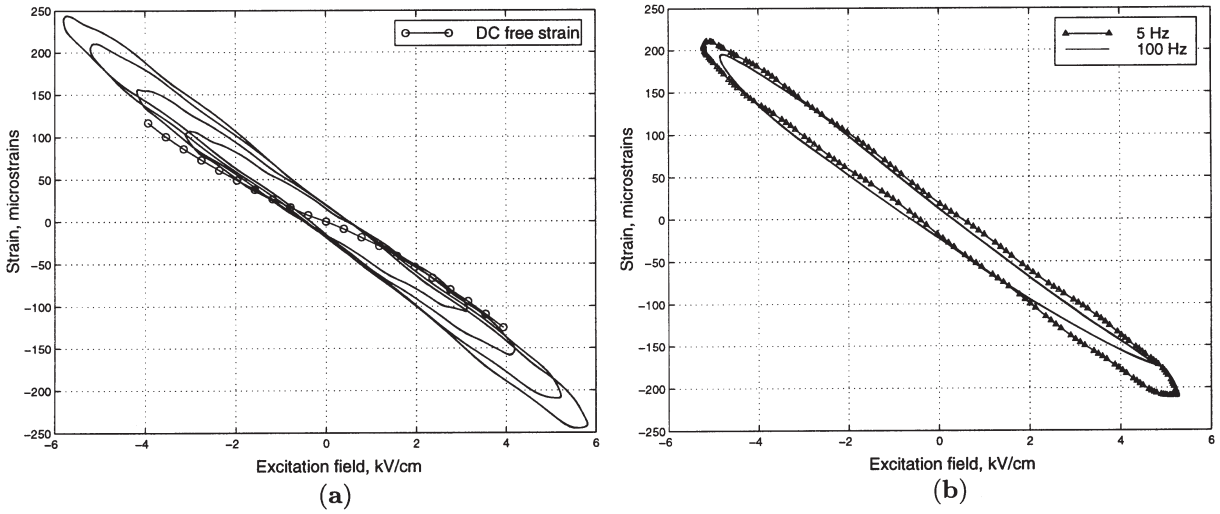

Figure 10. *Variation of strain hysteresis with field and frequency for a free actuator: (a) effect of increasing field, 5 Hz and (b) effect of increasing frequency.*

carried out at different excitation fields to see the effect of excitation field as well as excitation frequency and these results are summarized in Figure 11. The dependence of crucial material properties such as e_{33}^{σ} and tan δ on the magnitude and frequency of the excitation can be calculated from the magnitude and phase of the current drawn by the actuator. These parameters are very important for predicting the power consumption of actuators bonded to a structure. From Figure 11(a), it can be seen that the free strain, and hence, d_{31}, is relatively independent of the actuation frequency. The slight increase seen at higher frequencies is due to an electro-mechanical resonance around 1 kHz. The influence of the resonant dynamics can be seen more clearly in Figure 11(b), which is a plot of the phase of the free strain. These dynamics, though important for a free actuator, are of less interest while investigating the performance of actuators bonded to a structure, where the dynamics of the parent structure is dominant. At low frequencies, the free strain increases by approximately 10% due to poling effects. At higher frequencies and excitation fields, nonlinear effects cause the free strain to increase by as much as 15% compared to the free strain in the linear region.

This variation can be described in terms of the following relation:

$$E = A\varepsilon + B\dot{\varepsilon} \tag{14}$$

where E is the excitation voltage in volts and ε is the free strain of the actuator in microstrain. By analogy with a mechanical spring-damper system, the coefficients A and B can be considered as an effective stiffness and damping respectively. The variation of this stiffness and damping with excitation voltage and field is calculated from the transfer function shown above and curves are fit through the data. The values of the stiffness and damping are shown in Figure 12.

It can be seen that the stiffness depends to a large extent on

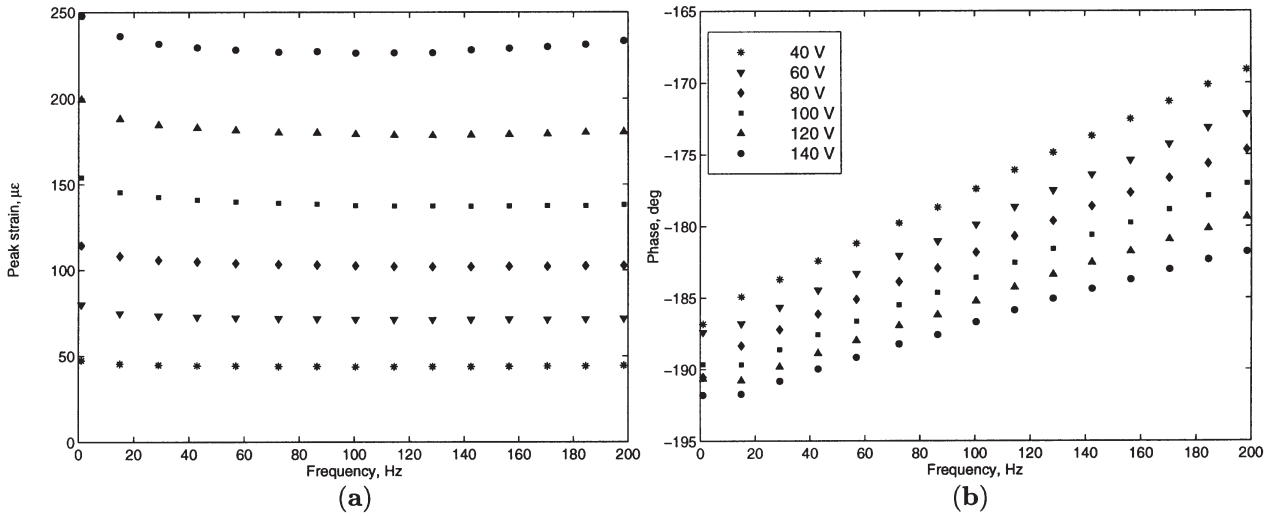

Figure 11. *Response of a free PZT actuator: (a) peak free strain and (b) strain phase.*

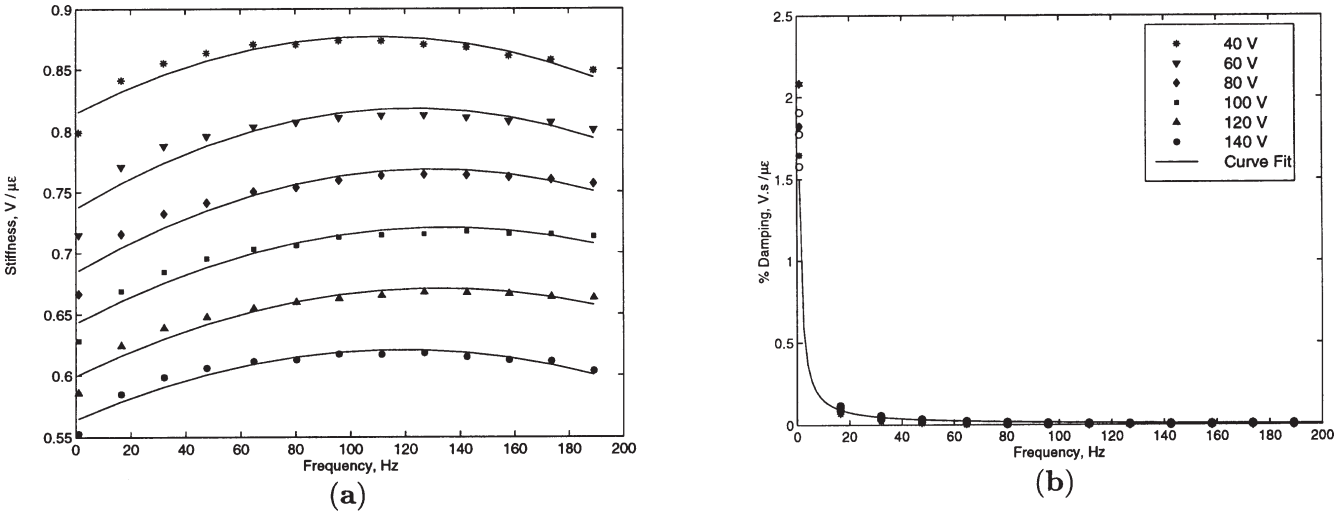

Figure 12. *Stiffness and damping variation: (a) effective stiffness coefficient* A *and, (b) effective damping coefficient* B.

excitation voltage, as expected, but the frequency dependence is small. A quadratic variation of stiffness with frequency is calculated and is given by

$$A = af^2 + bf + c \tag{15}$$

where f is the frequency of excitation in Hertz, and the coefficients a, b and c are linear functions of the excitation voltage.

$$a = 15.1\times10^{-9}E - 6.09\times10^{-6} \tag{16}$$

$$b = -2.59\times10^{-6}E + 1.4\times10^{-3} \tag{17}$$

$$c = -2.44\times10^{-3}E + 0.893 \tag{18}$$

The variation of damping with field is not significant, especially at higher values of frequency, so the damping is expressed as:

$$B = \frac{1.5}{f} \tag{19}$$

This expression for damping is equivalent to stating that the energy lost per cycle per unit displacement amplitude is a constant, which is intuitively expected. Using these relations for effective stiffness and damping, the free strain of the actuator can be calculated at any given frequency in the range of 1–200 Hz and excitation voltage in the range 40–140 V. The comparision of experimentally measured free strain with predictions using this phenomenological model is shown in Figure 13, where the sample is excited at 80 V_{peak} and 120 V_{peak} at frequencies of 5 Hz, 25 Hz and 100 Hz. It can be seen that at lower frequencies, the damping is underpredicted and at higher frequencies, the damping is overpredicted. This is due to the rather simple hyperbolic variation of the effective damping parameter assumed in Equation (19). A more complicated variation would yield more accurate results, but the accuracy of the present assumption is considered to be within acceptable limits.

It is worth mentioning here that the static free strain values can be obtained from the above equations by first setting $\dot{\varepsilon} = 0$ and then setting $f = 0$. The resulting equation for static free strain is

$$\varepsilon_{static} = \frac{E}{-2.44\times10^{-3}E + 0.893} \tag{20}$$

The values of static free strain obtained by this equation are very close to the values obtained from Equation (8), though not completely the same. This is because Equation (8) represents the static behavior which has an inherent asymmetry between positive and negative excitation voltages due to remnant polarization effects. This asymmetry decreases as the frequency of excitation increases. However, the model represented by Equation (14) assumes a solution which is inherently symmetric. Therefore, for static and low frequency behavior, Equation (8) should be used to obtain more accurate results while Equation (14) should be used for high frequency behavior.

Effect of DC Bias

Several researchers have reported the beneficial effects of operating piezoceramic actuators with a DC bias field. According to Kreuger (1967), a DC bias field increases the value of d_{31} under stress. Li et al. (1991) attribute the stabilizing effect of the DC bias to pinning of the domains. The domains are better aligned under a DC bias and the domain walls become more difficult to move, which effectively reduces the extrinsic contribution to non-linear effects and losses in actuation. Figure 14 shows a strain-field hysteresis

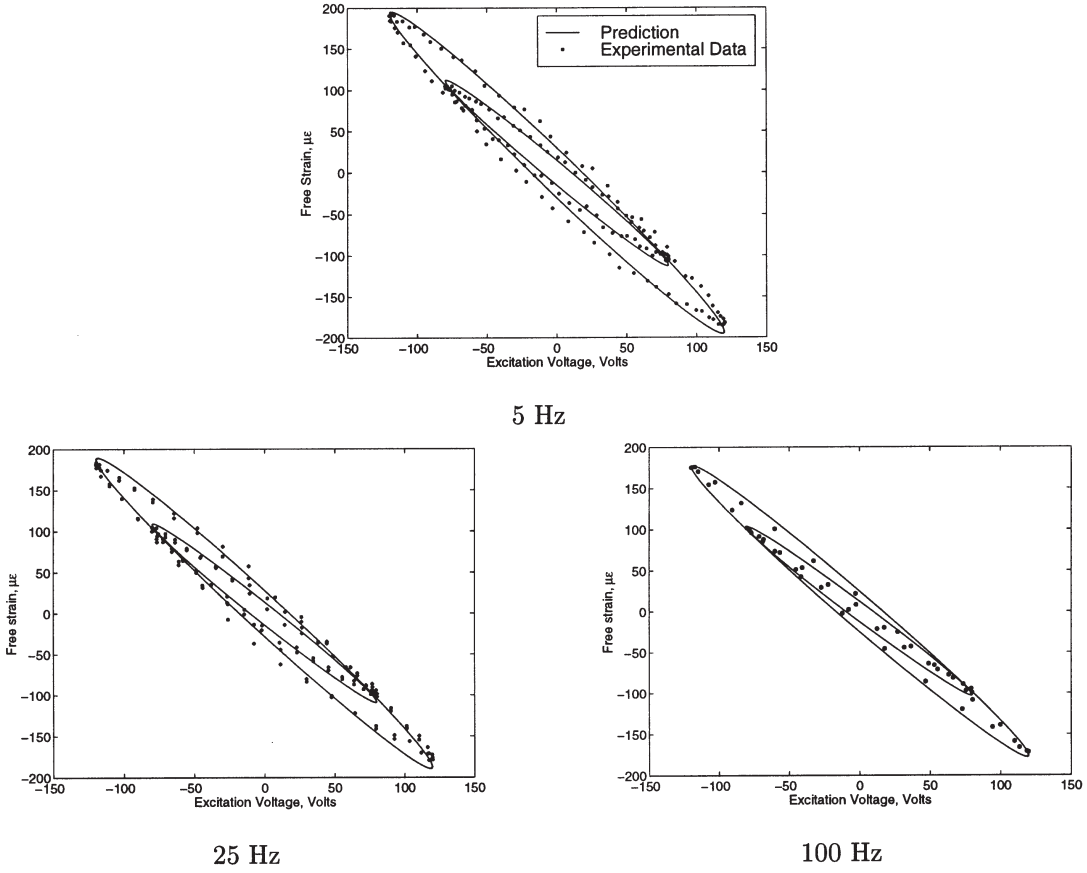

Figure 13. *Model validation at three different frequencies and two excitation voltages of 80* V_{peak} *and 120* V_{peak}.

loop under a pure AC field and under the same AC field with a superimposed positive DC field of strength 0.5 V_{peak}. Only the AC component of the strain is plotted for comparison. It can be seen that the area under the loop is less for the actuation with a bias than without bias. This shows that the losses have decreased due to the application of a DC bias. There is also a small decrease in the magnitude of peak free strain under bias.

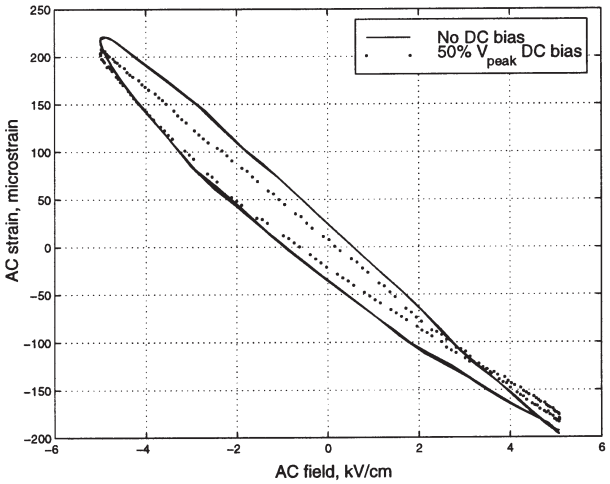

Figure 14. *Effect of a DC bias field.*

POWER CONSUMPTION

The prediction of power consumed by the system with bonded piezoactuators is a very important part of the design process. It is well known that the dielectric permittivity and the dissipation factor of piezoceramics increase with increasing field (Woollett and LeBlanc, 1973). This information is essential for predicting the power consumption of systems incorporating piezoceramic actuators. For PZT-5H, these variations were calculated from the current consumption measurements in the experiments described above.

For an ideal capacitor, the electrical impedance is given by:

$$Z = \frac{1}{j\omega C} \tag{21}$$

where ω is the angular frequency of the applied field and C is the capacitance in Farads, which for an ideal parallel plate capacitor is given by:

$$C = \frac{\varepsilon A}{t} \tag{22}$$

where ε is the dielectric permittivity, A is the area of the plate

and t is the distance between the plates, which in this case is the thickness of the piezoceramic sheet. If a sinusoidal voltage is applied to the capacitor, the current drawn leads the voltage by exactly 90°. Real capacitors with dielectric media, however, have energy losses. These losses are due to conduction currents in the dielectric as well as molecular friction opposing the rotation of dielectric dipoles. This causes the current to lead the voltage by a phase angle δ less than 90°. The non-ideal capacitor is usually modelled by a simplified equivalent circuit incorporating a shunt resistance in parallel with an ideal capacitor. The energy losses appear as ohmic heating in the shunt resistance. The dissipation factor, given by tan δ, is therefore a measure of the energy loss in the capacitor and consequently, the power consumed by the actuator. The impedance of a non-ideal capacitor can be given in terms of a complex dielectric permittivity (Matsch, 1964).

$$\bar{\varepsilon} = \varepsilon_o k' - j\varepsilon_o k'' = \varepsilon - j\varepsilon \frac{k''}{k'} \tag{23}$$

where ε_o is the permittivity of free space, k′ is the relative permittivity of the dielectric and

$$\tan\delta = \frac{k''}{k'} \tag{24}$$

From Equations (22), (23) and (24), the electrical impedance of the piezoceramic sheet can be expressed as:

$$Z = \frac{t}{j\omega e_{33}^{\sigma}(1 - j\tan\delta)A} \tag{25}$$

The experimentally measured current drawn and the calculated dissipation is shown in Figure 15. Equating the impedance from Equation (25) to the value of impedance calculated from the experimentally measured voltage and current, the variation of e_{33}^{σ} and tan δ with field can be generated and is shown in Figure 16. Curves are fit to the experimental data, and the variation of e_{33}^{σ} and tan δ with field can be calculated as:

$$K_e = 5.3187E^2 - 5.9754E + 7.32 \tag{26}$$

$$\tan\delta = 0.0662E + 0.0376 \tag{27}$$

where K_e is the percent increase in e_{33}^{σ} and E is the electric field in kV_{rms}/cm.

The power consumed by actuators bonded onto a beam is predicted by the impedance method (Liang et al., 1993), a short description of which is given here. The structural impedance of the active system is derived by considering a PZT actuator deforming along its length only, driving a single degree of freedom spring mass damper system. For an actuator of length l_c width w_c and thickness t_c, and with an elastic modulus Y_{22}^{E}, the force exerted is given by

$$F = K_A l_c(\varepsilon_{mech} - \Lambda) \tag{28}$$

where K_A is the static stiffness of the PZT, given by $Y_{22}^{E} w_c t_c / l_c$, Λ is the free strain which is defined as $d_{31}V/t_c$, and ε_{mech} is the mechanical strain of the structure at the actuator location. For a PZT being excited along the 3-axis (or z-axis) and assuming it deforms only along the 1-axis (or x-axis), the constitutive relations [Equations (1) and (2)] can be rewritten as:

$$\varepsilon_1 = \bar{s}_{11}^{E}\sigma_1 + d_{31}E \tag{29}$$

$$D_3 = \bar{e}_{33}^{\sigma}E + d_{31}\sigma_1 \tag{30}$$

in these equations, ε_1 is the strain, T_1 is the stress and $\bar{s}_{11}^{E}$ is the complex compliance. The equation of motion for a PZT vibrating in the x-direction is given by:

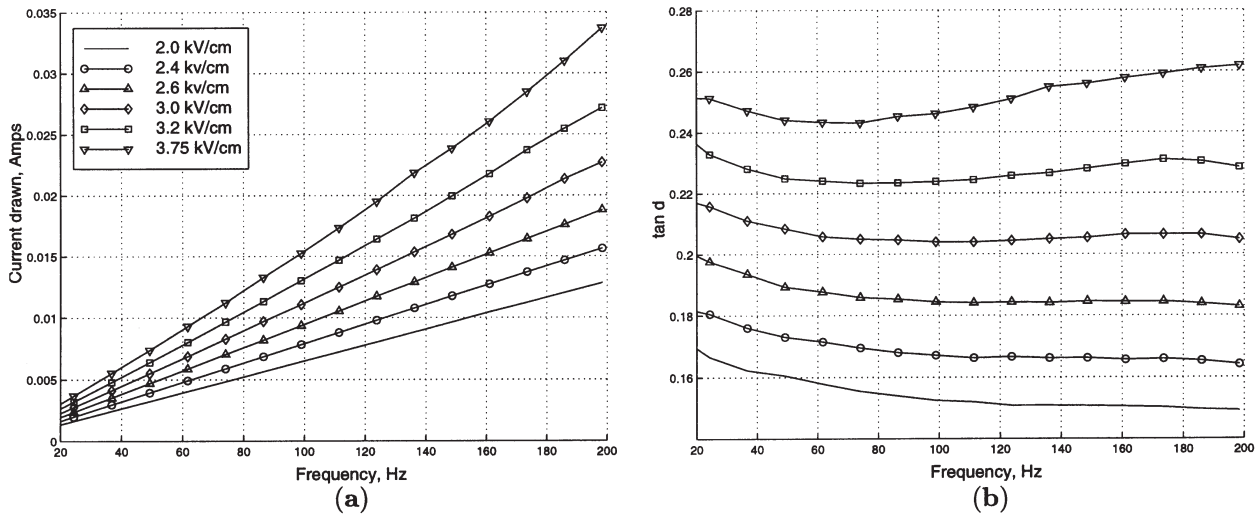

Figure 15. *Experimentally measured current and tan δ: (a) current drawn and (b) calculated tan δ.*

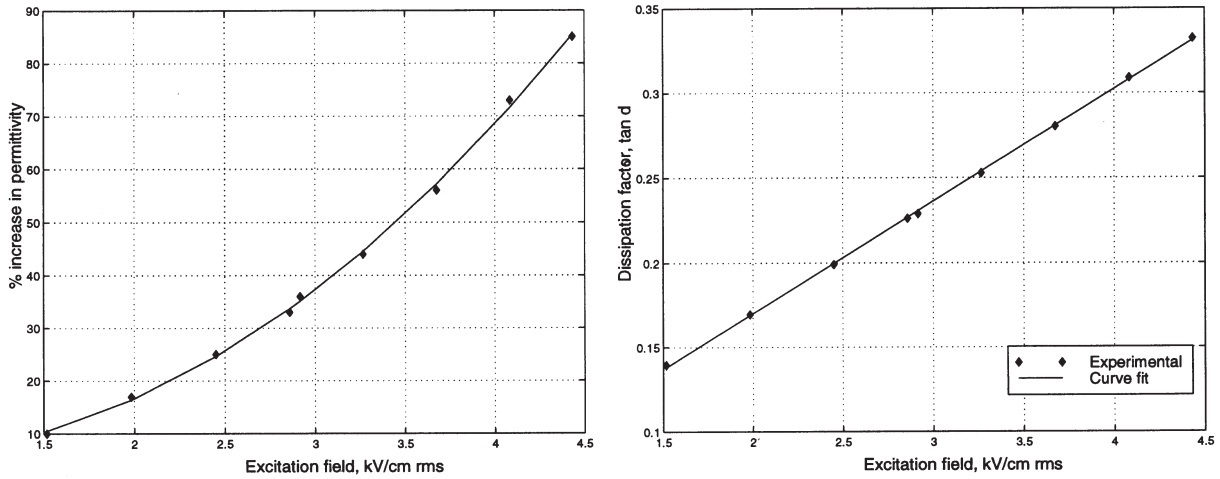

Figure 16. *Variation in coefficients with field: (a) dielectric constant and (b) dissipation factor.*

$$\rho \frac{\partial^2 u}{\partial t^2} = \bar{Y}_{11}^E \frac{\partial^2 u}{\partial x^2} \tag{31}$$

where $\bar{Y}_{11}^E$ is the complex modulus given by:

$$\bar{Y}_{11}^E = Y_{11}^E (1 + j\eta) \tag{32}$$

where η is the mechanical loss factor of the PZT. The complex dielectric permittivity $\bar{e}_{33}^{\sigma}$ is given by:

$$\bar{e}_{33}^{\sigma} = e_{33}^{\sigma}(1 - j\delta) \tag{33}$$

Assuming a solution to Equation (31) of the form

$$u = (a_1 \sin kx + a_2 \cos kx) e^{j\omega t} \tag{34}$$

where $k^2 = \omega^2 \rho / \bar{Y}_{11}^E$, and applying the appropriate boundary conditions, it is possible to derive expressions for constants a_1 and a_2. A similar derivation can be performed to find the impedance of an actuator (assuming both electrodes shorted) under a constant force excitation. This gives an actuator mechanical impedance expressed as:

$$Z_A = -\frac{K_A(1 + \eta j) kl_c}{\omega \tan(kl_c)} j \tag{35}$$

The mechanical impedance of the structure is defined as:

$$F = Z\dot{x} \tag{36}$$

Using the expressions for the mechanical impedances of the actuator and the structure, and using the derived constants a_1 and a_2, the assumed displacement [Equation (34)] can be solved for. This is then substituted in the constitutive relations [Equations (29) and (30)] to obtain the value of the electric displacement D_3. The current is defined as:

$$I = \dot{q} = j\omega \int\int D_3 dx dy \tag{37}$$

The final expression for the consumed current is:

$$I = j\omega E w_c l_c \left(\frac{d_{31}^2 \bar{Y}_{11}^E Z_A \tan(kl_c)}{(Z + Z_A) kl_c} + \bar{e}_{33}^{\sigma} - d_{31}^2 \bar{Y}_{11}^E \right) \tag{38}$$

Note that for a free PZT actuator, though the actuator impedance Z_A is finite, the impedance of the structure, Z is zero. Also, the factor $\tan(kl_c)/(kl_c)$ is approximately equal to unity. The current drawn by the free PZT [Equation (38)] then reduces to:

$$I_{freePZT} = j\omega E w_c l_c \bar{e}_{33}^{\sigma} \tag{39}$$

from this, the impedance of the free PZT can be written as

$$Z_{freePZT} = \frac{V}{I_{freePZT}} = \frac{t_c}{j\omega E w_c l_c \bar{e}_{33}^{\sigma}} \tag{40}$$

Note that this expression for the impedance of the free PZT is the same as the expression derived considering the PZT to be a lossy capacitor [Equation (25)], considering $\tan\delta \approx \delta$. The experimentally measured current consumed by a free actuator and a pair of actuators bonded to a beam is compared with that predicted using Equation (38). The variation of e_{33}^{σ} and $\tan\delta$ given by Equations (26) and (27) is also incorporated in the theoretical predictions. The mechanical impedance of the beam in bending [from Equation (36)] is given by:

$$Z = \frac{4}{(t_b + t_c)^2} \frac{M}{(\theta_2 - \theta_1) j\omega} \tag{41}$$

where M is the actuation moment, θ_2 and θ_1 are the beam slopes at the ends of the actuator and t_b is the beam thickness.

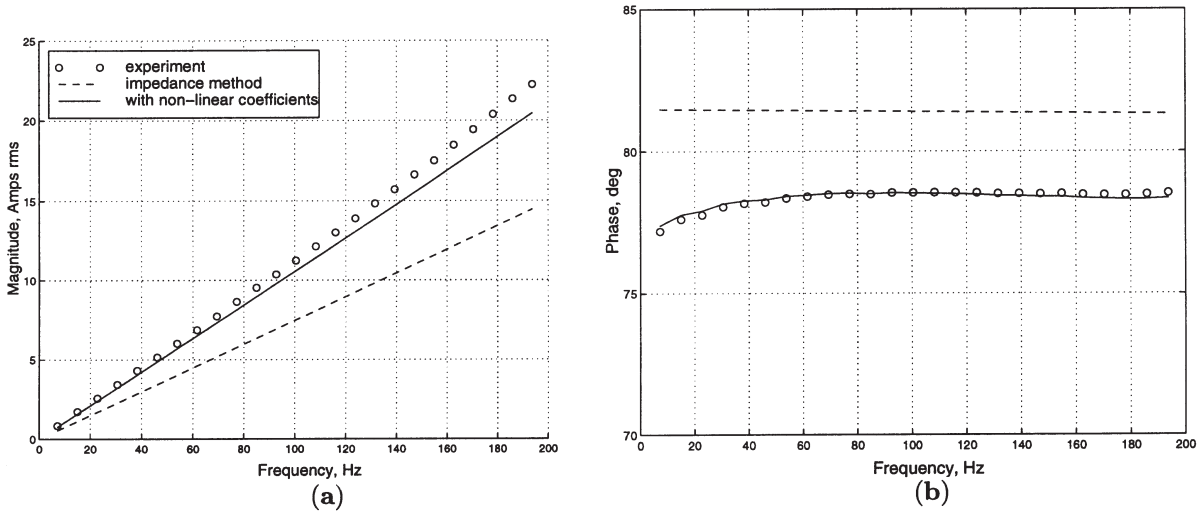

Figure 17. *Current consumption predictions for a free actuator, 3.0 kV_{rms}/cm: (a) magnitude of current and (b) phase.*

In the theoretical validation, the actuation moment M and the beam slopes θ_1, θ_2 are calculated using the Euler-Bernoulli model. Experiments were performed on a free actuator and on a pair of actuators bonded to a cantilevered aluminum beam of dimensions $12'' \times 1'' \times 0.032''$. The comparison of experimental and theoretically predicted current consumption is shown in Figures 17 and 18. The predicted values show very good agreement with experiment when the variation of e_{33}^{σ} tan δ is taken into account, and the agreement is poor when these parameters are assumed constant. This emphasizes the importance of incorporating these nonlinearities when attempting to predict the power consumption of such actuator systems.

DEPOLING BEHAVIOR

When exposed to a high electric field opposite to the poling direction, the piezoceramic loses most of its piezoelectric capability. The actuation is accompanied by large dielectric losses and poor efficiency. This is known as depoling of the piezoceramic and is accompanied by a permanent change in dimensions of the sample. This is probably due to large scale domain switching in the material. The DC depoling field of PZT-5H is approximately 5.5 kV/cm. For an AC excitation, the depoling field depends on the frequency. It is observed that under a dynamic excitation, the depoling field of the actuator becomes lower than the DC value. This trend is shown in Figure 19. As in other experiments, there is a relatively large scatter because of variations in the samples and their previous excitation history. A curve was fit to the experimental variation of depoling field with frequency.

$$E_{dep} = 2.292 \times 10^{-5} f^2 - 1.255 \times 10^{-2} f + 5.6 \qquad (42)$$

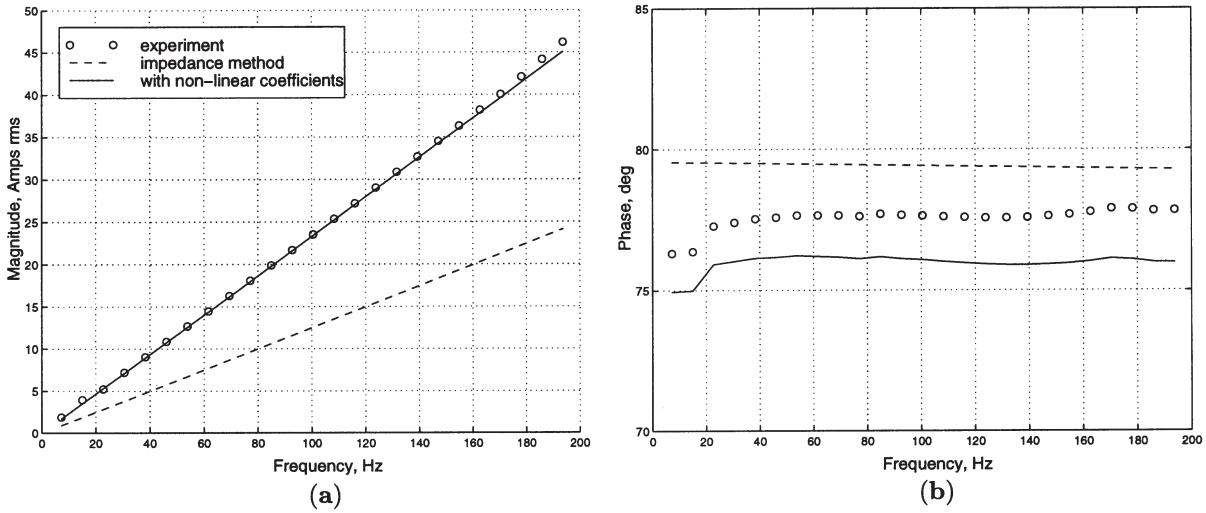

Figure 18. *Current consumption predictions for a pair of actuators bonded onto a beam, 3.0 kV_{rms}/cm: (a) magnitude of current and (b) phase.*

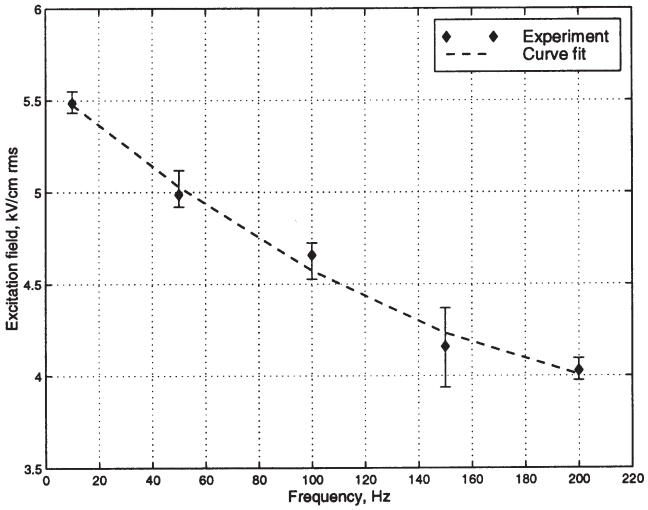

Figure 19. *Variation of depoling field with frequency.*

where E_{dep} is the AC rms depoling field in kV/cm and f is the excitation frequency in Hertz. Figure 20(a) shows the effect of depoling on the actuator strain response. The PZT is excited at 4.7 kV_{rms}/cm at 100 Hz. This is just at the depoling field, and the PZT usually takes a few seconds to depole, during which the strain-field hysteresis loop transforms slowly into the "butterfly loop" which indicates that the sample has depoled. This process is accompanied by a rapid increase in current drawn. It can be seen that the area under the depoled loop is more than the area under the non-depoled loop which indicates that the energy losses are much larger in the case of the depoled actuator.

However, the application of an electric field along the initial direction of polarization reorients the domains along the poling direction, thus reversing the depoling action. The sample was depoled and then repoled by exposing it to a DC electric field of 5.9 kV/cm and 7.1 kV/cm for about 5 minutes. The free strain curves before and after repoling are shown in Figure 20(b). Though these repoling fields are much less than the initial poling field of the ceramic, which is usually of the order of 12 kV/cm, it is possible to recover most of the performance of the actuator. This may be useful in case of accidental depoling of actuators in smart systems. It was also observed that it is possible to repole the samples by means of exciting it with an AC field that is approximately 90% of the AC depoling field. An interesting observation during this kind of repoling is that after the actuator has depoled, it is necessary to shut off the excitation and let the actuator sit for 3–4 minutes before applying the repoling field. If this is not done, the repoling is not effective. Note that it is more difficult to repole actuators bonded onto structures since the tensile stresses created in the actuator by the application of the repoling field tend to impede domain reorientation. Care should be taken not to exceed the tensile failure stress of the piezoceramic, which will result in cracking of the bonded actuator.

CONCLUSIONS

The behavior of a commercially available piezoceramic sheet actuator was investigated under different kinds of excitation as well as external loading. The power consumption of both free and surface bonded actuators was measured and compared with theoretical predictions. Response to excitation with a DC bias, depoling behavior, repoling effectiveness and drift were also investigated. The following conclusions summarize the results of this work.

1. The effect of compressive stresses is well known and usually decreases the actuator performance. The effect of tensile stresses perpendicular to the direction of poling is small and increases the free strain of the actuator. An external tensile stress of 2500 psi causes an increase in the actuator free strain of the order of 10% at an excitation field of 3.937 kV/cm. However, during the design of smart

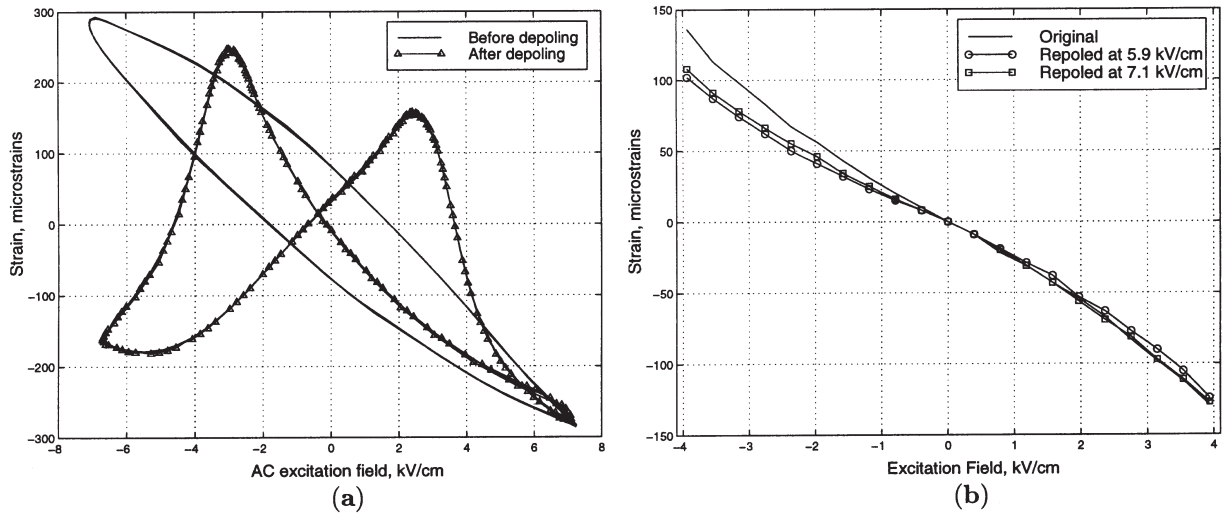

Figure 20. *Depoling behavior: (a) comparison of depoled and non-depoled strain response and (b) repoling effectiveness.*

systems, it is advisable to keep the stresses on the actuator to a minimum in order to obtain the best performance. Tensile stresses should especially be avoided since the ceramic is quite weak in tension.

2. Design of the actuator for use in DC applications has to take into account the drift phenomenon, which can be as high as 15% for moderately high fields. It appears possible to stabilize the drift by exposing the actuator to higher DC fields before the actual excitation.
3. A phenomenological model of the PZT free strain analogous to a mechanical single degree of freedom spring damper system is developed and validated experimentally.
4. It is possible to predict the power consumption of free and surface bonded actuators fairly accurately using the impedance method, given the variation of the dielectric permittivity and dissipation factor with field for a free actuator. Once these variations are known for a specific actuator, and an expression for the mechanical impedance of the structure is obtained, the current drawn by the actuators bonded on the structure can be predicted. The accuracy of the prediction becomes lower at high values of field and frequency. Discrepancies are noticable for fields above 4.8 kV_{rms}/cm and frequencies above roughly 100 Hz due to non-linearities.
5. A DC bias is beneficial during the AC operation of the actuators, since it reduces losses in the actuator. The application of a DC bias during actuation offers the added advantage of operating without as much danger of depoling the material as in a pure AC application.
6. Depoling of the actuators is a major problem in smart systems, especially since the depoling field decreases with excitation frequency. It is possible to repole the actuators by application of a positive DC field or an AC field. The recommended repoling technique is the application of an AC field along with a large positive DC bias. It should however be noted that while repoling actuators bonded onto structures, tensile stresses are induced in the actuator which might cause it to crack if the repoling field is too high. In such cases, repoling with an AC field along with a smaller DC bias may be appropriate.

ACKNOWLEDGEMENTS

This work was sponsored by the army research office under grant DAAH-04-96-10334 with Dr. Gary Anderson serving as technical monitor.

REFERENCES

IEEE Standard on Piezoelectricity. 1987. ANSI/IEEE., Std. 176.

Morgan Matroc Inc. Piezoceramic Databook. 1993. Morgan Matroc Inc., Electroceramics Division.

1997. *Physik Instrumente (PI) Catalog, US-edition,* Physik Instrumente (PI).

Brown, R. F. 1961. "Effect of two-dimensional mechanical stress on the dielectric properties of poled ceramic barium titanate and lead zirconate titanate," *Canadian Journal of Physics,* 39:741–753.

Chen, P. C. and Chopra, I. 1997. "Hover Testing of Smart Rotor with Induced-Strain Actuation of Blade Twist," *AIAA Journal,* 35(1).

Chopra, I. 1996. "Review of Current Status of Smart Structures and Integrated Systems," *SPIE Smart Structures and Integrated Systems,* 2717:20–62.

Chopra, I. 1997. "Status of Application of Smart Structures Technology to Rotorcraft Systems," *Presented at the Innovations in Rotorcraft Technology, Royal Aeronautical Society, London,* 2717:20–62.

Gerson, R., Burlage, S. R. and Berlincourt, D. 1961. "Dynamic tensile stress of a Ferroelectric ceramic," *Journal of the Acoustical Society of America,* 33(11):1483–1485.

Kreuger, H. H. A. 1967. "Stress sensitivity of piezoelectric ceramics, Part 1: Sensitivity to compressive stress parallel to the polar axis," *Journal of the Acoustical Society of America,* 42(3):636–645.

Kreuger, H. H. A. 1968. "Stress sensitivity of piezoelectric ceramics, Part 3: Sensitivity to compressive stress perpendicular to the polar axis," *Journal of the Acoustical Society of America,* 43(3):583–591.

Kreuger, H. H. A. and Berlincourt, D. 1961. "Effects of high static stress on the piezoelectric properties of transducer materials," *Journal of the Acoustical Society of America,* 33(10):1339–1344.

Li, S., Cao, W. and Cross, L. E. 1991. "The extrinsic nature of nonlinear behavior observed in lead zirconate titanate ferroelectric ceramic," *Journal of Applied Physics,* 69(10):7219–7224.

Liang, C., Sun, F. and Rogers, C. A. 1993. "Coupled electro-mechanical analysis of piezoelectric ceramic actuator driven systems—determination of the actuator power consumption and system energy transfer," *Proceedings of the SPIE Smart Structures and Intelligent Systems Symposium,* 1917:286–298.

Matsch, L. W. 1964. *Capacitors, Magnetic Circuits and Transformers,* Prentice-Hall Inc.

Vigness, I. 1935. "Dilatations in Rochelle Salt," *Physical Review,* 48:198–202.

Woollett, R. S. and LeBlanc, C. L. 1973. "Ferroelectric Non-linearities in transducer Ceramics," *IEEE Transactions on Sonics and Ultrasonics,* SU-20(1):24–31.

Zhang, Q. M., Zhao, J., Uchino, K. and Zheng, J. 1997. "Change of the weak-field properties of $Pb(Zr,Ti)O_3$ piezoceramics with compressive uniaxial stresses and its links to the effect of dopants on the stability of the polarizations in the materials," *Journal of Materials Research,* 12(1):226–234.